How HST/WFC3 and JWST can measure Galaxy Assembly and AGN growth

Rogier A. Windhorst and Seth H. Cohen

School of Earth & Space Exploration, Arizona State University, Tempe, AZ 85287-1404, USA

Abstract.
Accretion disks around Supermassive Black-Holes (SMBH's) in the centers of galaxies cause Active Galactic Nuclei (AGN), which are observable over the entire electromagnetic spectrum and out to the beginning of galaxy formation. The gradual assembly of galaxies is believed to have resulted in SMBH's today. The growth of SMBH's is largely hidden by dust, and possibly by large time-delays between galaxy mergers and the feeding of the central monster, so that the connection between galaxy assembly and SMBH-growth is currently at best circumstantial. Facilities like HST WFC3 and JWST are needed to trace this process from the epoch of reionization to the present.

Using panchromatic deep HST WFC3+ACS imaging data, grism spectra, and ground-based spectroscopy in GOODS and the HUDF, we address this issue through the epoch dependent rate of major mergers in massive galaxies in the HUDF, and through SED-fitting of objects with and without (known) AGN in GOODS. On average, the field galaxy population at z=1–6 has an underlying star-forming SED with typical ages of 0.1–0.2 Gyr. However, most AGN-dominated objects at z=0.5–1.5 have an underlying stellar SED age of $\sim$1 Gyr on average. This suggests that AGN growth/SMBH-feeding may become visible about 0.5–1 Gyr *after* the dynamical event which triggers the dominant starburst at these redshifts. This may also be reflected in the peak in the massive galaxy major merger-rate, compared to the peak in the redshift distribution of weak AGN. Finally, we discuss how the James Webb Space Telescope will expand on this topic in the next decade from the epoch of First Light to the present.

Keywords: Galaxy Assembly, AGN Growth, Hubble WFC3, James Webb Space Telescope

INTRODUCTION

From the WMAP polarization results (Kogut et al. 2003; Komatsu et al. 2010), population III stars likely existed at z$\simeq$20. These massive stars ($\gtrsim 250 M_\odot$) are expected to produce a large population of black holes (BH; $M_{bh} \gtrsim 150 M_\odot$; Madau & Rees 2001). Since there is now good dynamical evidence for the existence of supermassive ($M_{bh} \simeq 10^6$–10^9 $M_\odot$) black holes (SMBH's) in the centers of galaxies at z$\simeq$0 (Kormendy & Richstone 1995; Magorrian, Tremaine, & Richstone 1998; Kormendy & Gebhardt 2001; Gebhardt 2010), it is important to understand how the SMBH's seen at z$\simeq$0 have grown from lower mass BH's at z$\simeq$20. A comprehensive review of SMBH's is given by Ferrarese & Ford (2004). One suggestion is that they "grow" through repeated mergers of galaxies which contain less massive BH's, so the byproduct is a larger single galaxy with a more massive BH in its center. The growth of this (SM)BH may then be observed via its AGN activity. If this scenario is valid, there may be an observable link between galaxy mergers and increased AGN activity (Silk & Rees 1998).

Recent numerical simulations addressed some long-standing issues in the dissipational collapse scenario by including previously-neglected energetic feedback from cen-

tral SMBH's during the merging events (e.g. Robertson et al. 2005). They emphasize the relationship between the central BH mass and the stellar velocity dispersion, which confirms the link between the growth of BH's and their host galaxies (di Matteo et al. 2005; Springel et al. 2005). In the comoving volume of a few Mpc^3 surveyed by the HUDF at redshifts z≃2–6, the universe contains on average $\sim10^{12-13}M_\odot$ in Dark Matter, $\sim2\times10^{11-12}M_\odot$ in baryons, $\sim2\times10^{10-11}M_\odot$ in stars inside galaxies, and about $\sim4\times10^{7-8}M_\odot$ in SMBHs. At z$\gtrsim$6, both galaxies and SMBHs in this volume reside in at least 100 different *small* objects. By z$\sim$0, these will have merged into a few *giant* galaxies today. It is therefore imperative to measure exactly how AGN-activity and SMBH-growth has proceeded along with the process of galaxy assembly.

Deep X-ray, radio and mid-IR surveys traditionally have been ways to sample weak AGN at cosmological distances. However, even the current deepest radio and X-ray surveys are not deep enough to trace SMBH-growth in the weakest AGN in faint galaxies. This paper will therefore focus on other ways to investigate to the relevant questions on this topic: (1) To what extent did the process of hierarchical galaxy assembly go hand-in-hand with SMBH-growth as traced by AGN activity?; (2) Was the epoch-dependent rate of (major or minor) mergers the main driver of SMBH growth, AGN activity, and also of galaxy assembly?; (3) What kind of time delay existed between these processes?; and (4) How can the new Hubble WFC3 and JWST best measure this?

GALAXY ASSEMBLY, MERGER-RATE, AND WEAK AGN VS. Z

One of the remarkable discoveries of HST was how numerous and small faint galaxies are (Abraham et al. 1996, Driver et al.1995, Glazebrook 1995). They are likely the building blocks of the giant galaxies seen today. Galaxies with types on the present-day Hubble sequence formed over a wide range of cosmic time, but with a notable phase transition around z≃1: (1) Subgalactic units rapidly merge from z≃7 to z≃1 to grow bigger units; (2) Merger products start to settle as galaxies with giant bulges or large disks around z≃1. These evolved mostly passively since then (e.g., Cohen et al. 2003), resulting in the giant galaxies that we see today. JWST can measure how galaxies of all types formed over a wide range of cosmic time, by accurately measuring their distribution over rest-frame type and structure as a function of redshift or cosmic epoch (Windhorst et al. 2006).

Earlier work in the Hubble Ultra Deep Field (HUDF) suggested that early-stage mergers (as traced by tadpole galaxies, Straughn et al. 2006) and weak AGN (as traced by faint variable objects, Cohen et al.2006) have redshift distributions similar to that of field galaxies, but there is very little overlap between the HUDF samples of early stage mergers and variable AGN. This suggests that SMBH-growth may have on average kept in pace with galaxy assembly, but with a time-delay of at least 1 Gyr since the last major merger, as recent models predict (di Matteo et al. 2005; Hopkins et al. 2005).

The new HST WFC3 recently provided — together with existing ACS data superb Early Release Science (ERS) images in GOODS-South in 10 filters (UV+UBViz+YJH) from 0.2–1.7μm with 0.07–0.15" FWHM resolution, reaching AB=26.5-27.0 mag (10-σ) over 40–50 arcmin^2 (Windhorst et al. 2010). The 10-band WFC3 ERS redshift estimates are accurate to $\sim$4% with small systematic errors (Cohen et al. 2010), resulting
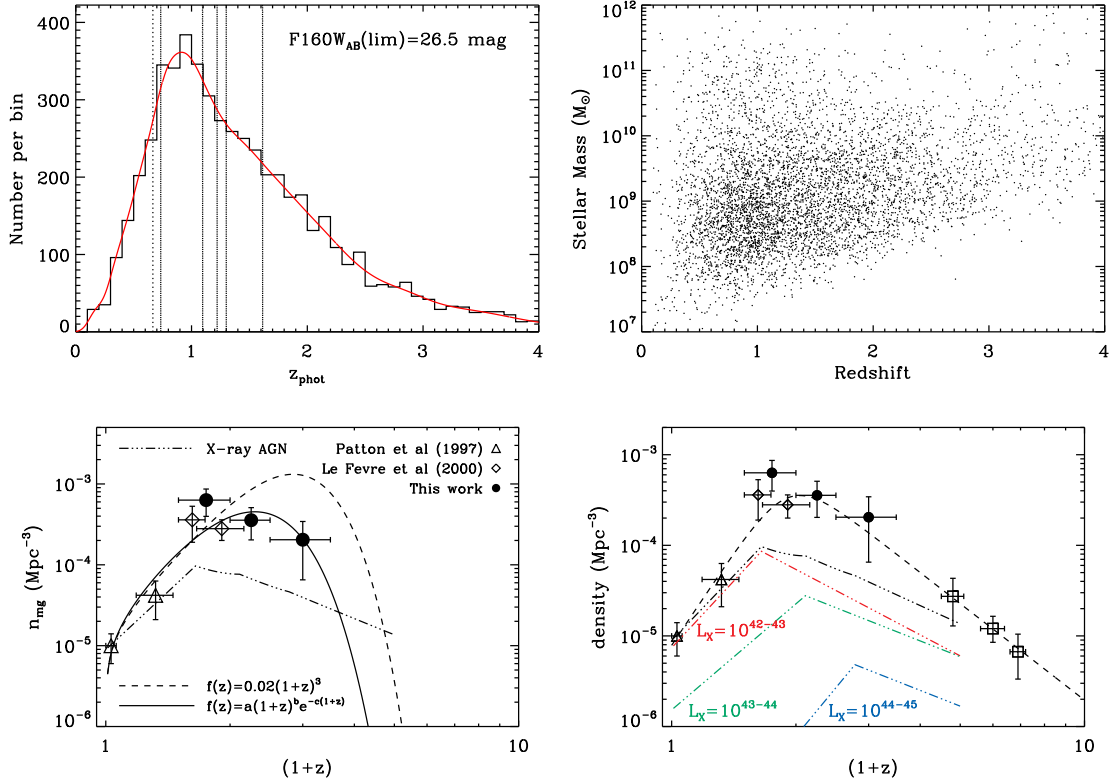
Fig. 1a–1b (Top) WFC3 ERS 10-band photometric redshift distribution and stellar mass vs. redshift (Cohen et al. 2010). Fig. 2ab (Bottom) Epoch dependent HUDF merger rate compared to X-ray selected luminosity density (Ryan et al. 2008).

in a reliable redshift distribution (Fig. 1a). This superb data set has enable us to do a number of new studies. Hathi et al. (2010) measured the luminosity function (LF) of Lyman Break Galaxies at the peak of cosmic star-formation ($z \simeq 1$–3), tracing its faint-end slope with redshift. Ryan et al. (2010) traced the mass assembly of early-type galaxies for $z \lesssim 4$. Reliable masses of faint galaxies to AB=26.5 mag (Fig. 1b) trace the process of galaxy assembly, downsizing, and merging, in order to connect these processed with weak AGN growth in the same objects.

An essential part of such a study is to measure the epoch-dependent galaxy major merger rate to AB $\lesssim 27$ mag. Ryan et al. (2008) measured the HST/ACS grism pair-fraction as a function of redshift in the HUDF. Their deep imaging and spectroscopic sample had broad-band point source completeness for $i_{AB} \lesssim 30.0$ mag and ACS grism point source completeness for $i_{AB} \lesssim 27.0$ mag (Ryan et al. 2007). Following Fig. 1b, the mass completeness limit for $z \lesssim 2$ from Bruzual & Charlot (2007) SED fitting is $M \gtrsim 10^{10.0} M_{\odot}$ for the primary galaxy mass, and $M \gtrsim 10^{9.4} M_{\odot}$ for the secondary galaxy mass in the pair. Ryan et al. (2008) selected major mergers with $0.25 \leq M_2/M_1 \leq 1$. Their sample has spectro-photometric redshifts (spz's) for both galaxies in the pair, and measured the epoch-dependent galaxy pair fraction for $z \lesssim 6$. Fig. 2a–2b compares the galaxy major merger density to the Chandra SDSS QSO density vs. redshift, the latter for various X-ray luminosity slices. Fig. 2b suggest that both have similar redshift distributions, but possible with a ~ 1 Gyr offset in cosmic time. This may support —
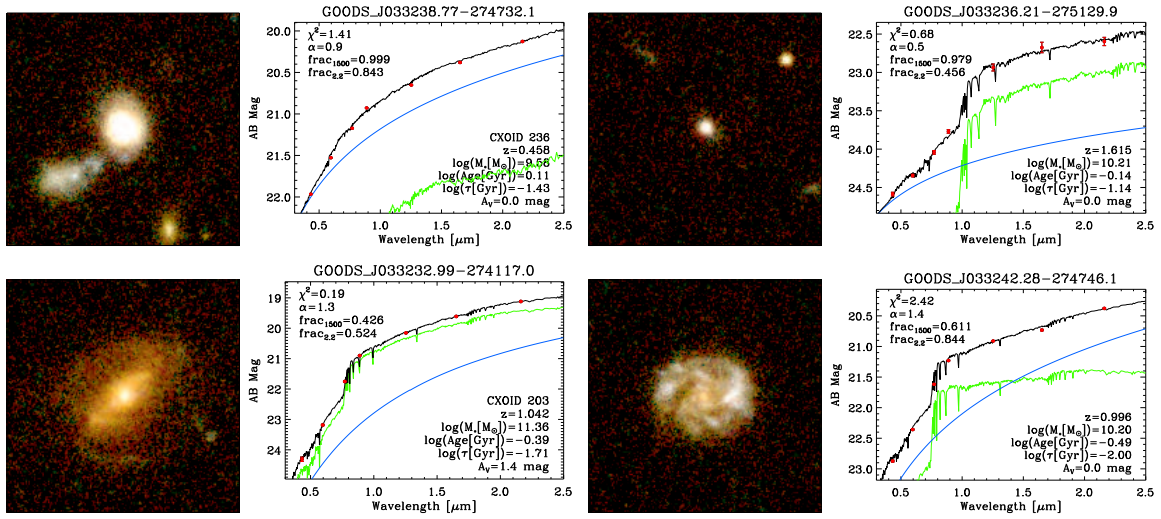
GOODS_J033238.77−274732.1

$\chi^2=1.41$
$\alpha=0.9$
$frac_{1500}=0.999$
$frac_{2.2}=0.843$

CXOID 236
$z=0.458$
$\log(M_*[M_\odot])=9.56$
$\log(Age[Gyr])=0.11$
$\log(\tau[Gyr])=-1.43$
$A_V=0.0$ mag

GOODS_J033236.21−275129.9

$\chi^2=0.68$
$\alpha=0.5$
$frac_{1500}=0.979$
$frac_{2.2}=0.456$

$z=1.615$
$\log(M_*[M_\odot])=10.21$
$\log(Age[Gyr])=-0.14$
$\log(\tau[Gyr])=-1.14$
$A_V=0.0$ mag

GOODS_J033232.99−274117.0

$\chi^2=0.19$
$\alpha=1.3$
$frac_{1500}=0.426$
$frac_{2.2}=0.524$

CXOID 203
$z=1.042$
$\log(M_*[M_\odot])=11.36$
$\log(Age[Gyr])=-0.39$
$\log(\tau[Gyr])=-1.71$
$A_V=1.4$ mag

GOODS_J033242.28−274746.1

$\chi^2=2.42$
$\alpha=1.4$
$frac_{1500}=0.611$
$frac_{2.2}=0.844$

$z=0.996$
$\log(M_*[M_\odot])=10.20$
$\log(Age[Gyr])=-0.49$
$\log(\tau[Gyr])=-2.00$
$A_V=0.0$ mag

Fig. 3. Cohen et al. (2010): Multi-band HST images and two-component SED fitting for GOODS objects with known VLT redshifts. Best fit Bruzual-Charlot (2003, 2007) stellar SEDs (green) plus a power-law AGN (blue) are shown, as well as their sum (black). Fig. 3a–3b (Top) show objects with (dominant) blue power-law AGN and Fig. 3c–3c (Bottom) show objects with (dominant) red power-law AGN.

— although given the quality of the current data — does not prove the hierarchical model predictions that there could be a ~1 Gyr time delay between the major merger and SMBH feeding, or the onset of the visible weak AGN. JWST will be able to do this work 3–5 mag fainter with AB≃31.5 mag (1 nJy) imaging at 0.05–0.2" FWHM resolution from 0.7–5.0 μm, and 0.2–1.2" FWHM at 5–29μm, sampling the rest-frame UV-optical and tracing young+old SEDs & dust for z≃0–20. Hubble's new WFC3 is thus an essential pathfinder at z≲8–9 for JWST at z≳9.

RADIO & X-RAY HOST SED-AGES: TRACING AGN GROWTH?

The unique 10-band (UVU+BViz+YJH) ERS data in GOODS-S was combined by Cohen et al.(2010) with ground-based VLT JHK photometry and VLT spectroscopic redshifts for objects with AB≲24–25 mag (Le Fèvre et al. 2004; Szokoly et al. 2004; Vanzella et al. 2005, 2008; see also www.eso.org/science/goods/spectroscopy/). For 1549 GOODS objects with *known* redshifts, Cohen et al. (2010) applied SED fitting for restframe wavelengths $0.12 \lesssim \lambda_{rest} \lesssim 1.6$ μm, using a combination of: (a) a Bruzual-Charlot (2007) stellar population model, and (b) an AGN power law $S_\nu \propto \nu^\alpha$ bluewards of the IR dust emission. For the typical field galaxy redshifts in this sample (z≃0.5-1.5, see Fig. 1a), the 10-band photometry brackets the Balmer and 4000Å breaks.

The two-component SED fitting uses the following ingredients: (1) solar metallicity and a Salpeter IMF, which is justified since most objects are at z≲2 (Fig. 1a); (2) n=16 e-folding times τ in a log-spaced time grid from 0.01-100 Gyr; (3) n=244 SED ages t≲ age of Universe at each redshift in WMAP-year7 cosmology (Komatsu et al.2010); (4) Calzetti et al. dust extinction with n=21 intervals covering $0 \lesssim A_V \lesssim 4.0$ mag in 0.2 mag steps; (4) n=16 power-law slope values $0 \lesssim \alpha \lesssim 1.5$ — as appropriate for UV-optical
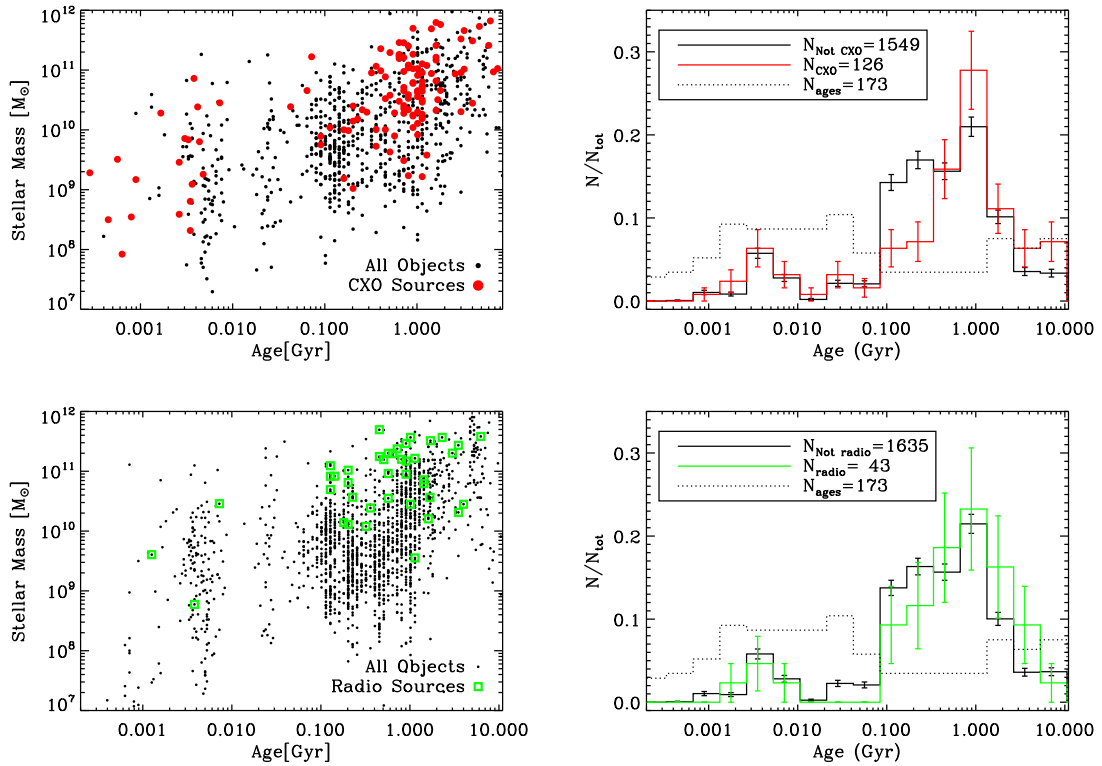
Fig. 4a–4b (Top). Red dots and histograms show the best fit stellar mass vs. SED age for X-ray selected objects in GOODS (Cohen et al. 2010). Fig. 4c–4d (Bottom) Green dots and histograms show the same for radio selected objects in GOODS. Black dots and full-drawn lines represent all 1549 GOODS objects with known redshifts. Dotted histograms show the input SED model ages used in the χ^2 fitting.

AGN — in steps of 0.1 in α. The two-component SED fitting yields $\sim 10^6$ models for the 1549 GOODS galaxies with known redshifts. The multi-parameter χ^2 surface is searched for best-fit SED type (τ) and SED age t, stellar mass M, plus possible AGN UV–optical power-law component slope α and amplitude (f_{AGN} defined at 1500Å or 2μm in the restframe). The χ^2 fitting method follows the concept of Windhorst et al. (1991, 1998), where HST and ground-based UBgriJHK images showed non-negligible weak AGN components in mJy radio galaxies. Fig. 3a–3b shows typical examples for objects where the SED fitting demands an additional *blue* component, which in the case of Fig. 3a is a clearly dominant blue power-law. Fig 3c–3d shows typical examples for objects where the SED fitting demands an additional *red* component, which in the case of Fig. 3d is a clearly dominant red power-law. Future work in progress covers other potential caveats of this method: (a) Young stellar populations may have power-law UV spectra (Hathi et al. 2008), which may tend to overestimate UV AGN power-law; (b) Include Spitzer IRAC data to model the 1–2 Gyr red AGB population to better trace any IR AGN power-laws; (c) Fit the BC07 stellar SED only to objects where χ^2 doesn't require both. Further details are presented in Cohen et al. (2010).

Fig. 4a–4b shows the best fit stellar mass vs. SED age for all X-ray selected objects in GOODS (red dots and histograms). Fig. 4c–4d shows the same for all radio selected
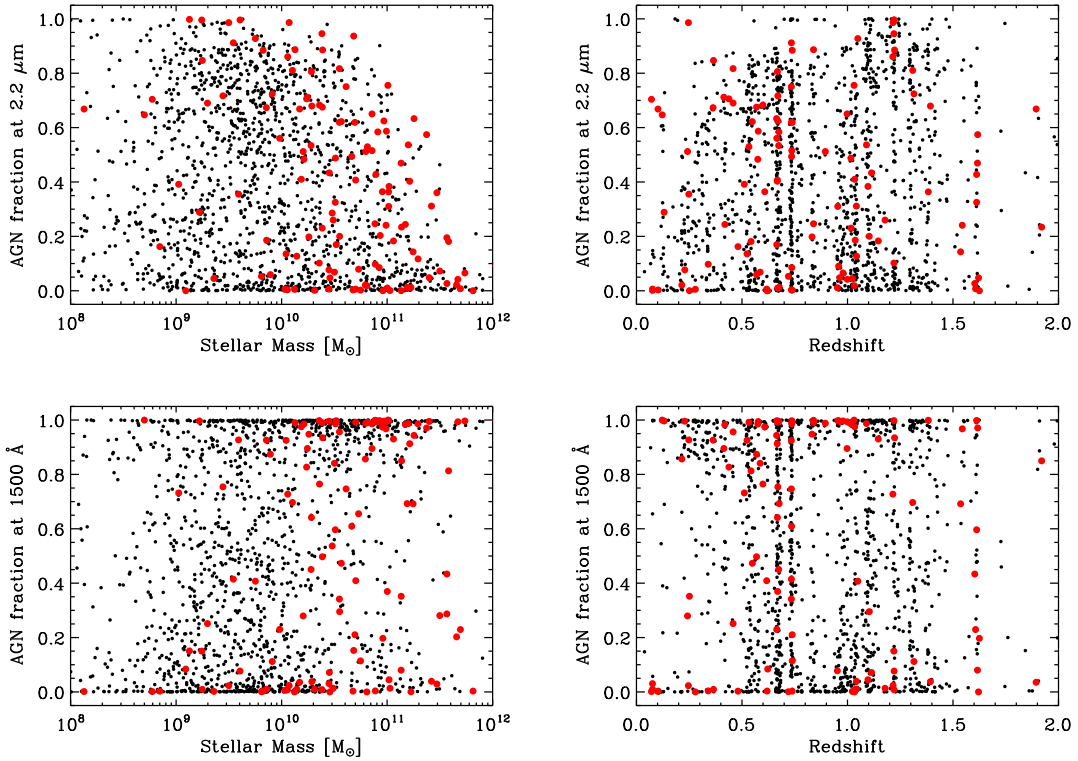
Fig. 5a–5d. Best-fit AGN fraction f_{AGN} at both 1500 and 2μm wavelength vs. stellar mass and redshift for X-ray selected objects (red) and all field galaxies (black) with known redshifts in GOODS (Cohen et al. 2010). The fraction of objects with a secondary blue SED component ($f_{AGN} \gtrsim 50\%$) is non-negligible at 1500 — at least the X-ray selected objects amongst those (red circles) host weak AGN.

objects (green dots and histograms). Black dots and black full drawn lines represent the GOODS field galaxies in all panels. The black dotted histograms show the input SED model ages used in the χ^2 fitting, which are fairly flat with log(age). Hence, the output field, radio and X-ray galaxy SED-ages were *not biased* due to the input model age distribution. Faint field galaxies occupy a "blue" cloud with typical age of $\sim$100-200 Myr, and a "red" cloud with typical age of $\gtrsim$ 1–2 Gyr. The histograms in Fig. 4b and 4d shows that weak X-ray and radio-selected AGN, respectively, reside in galaxies that are a bit older than the general field galaxy population, but by no more than $\lesssim$ 0.5–1 Gyr on average. A smaller fraction of the weak X-ray and radio-selected AGN coincides with blue starforming field galaxies with ages of 0.1–0.2 Gyr. A small but not entirely negligible fraction of the X-ray selected object also coincides with very young field galaxies with ages $\lesssim$ 50 Myr. We believe these are X-ray sources associated with X-ray binary populations in lower redshift actively starforming galaxies.

Fig. 5a–5d shows the AGN fraction f_{AGN} at restframe wavelength of 1500Å and 2μm vs. stellar mass and redshift for faint X-ray selected objects (red) and field galaxies (black) in GOODS (Cohen et al. 2010). For a non-negligible fraction of the X-ray selected Type-1 AGN more than 50% of the 1500Å-flux appears to come from the AGN. This is true to a lesser extend for the 2μm-flux as well. In both cases, there seems
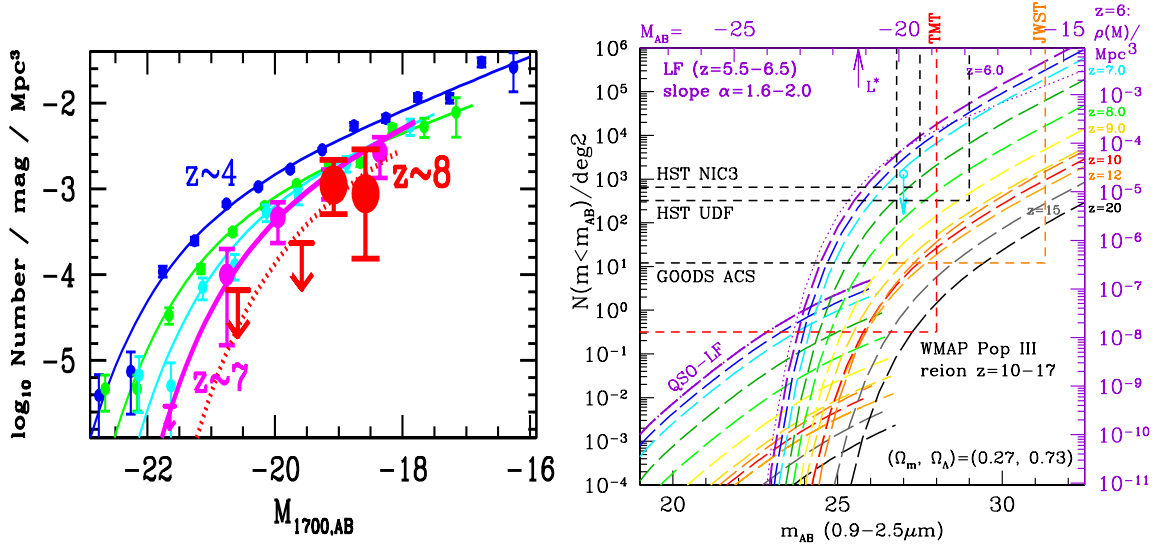
Fig. 6a (left) The LF of HUDF and GOODS objects at z≃4–8 (Bouwens et al. 2010, Yan et al.2009). Fig. 6b (right) Extrapolation of the Yan et al. (2004b, 2009) z=6 LF — including those for QSOs — as expected for z=7–20 for JWST (see Windhorst et al. 2006).

to be a population of faint field galaxies (black dots) which also have a non-negligible f_{AGN} fraction. If not due to a secondary blue *stellar* SED component, many more such very weak AGN are currently too faint to be detected by Chandra or the VLA, but can be detected by future X-ray or radio facilities such as IXO or SKA. JWST will be able to disentangle multiple SED + AGN power-law components from 15-band photometry to AB ≲ 31 mag, tracing AGN-growth and host galaxy masses from SED-ages and AGN fractions for M ≳ $10^8 M_\odot$ and z ≲ 10.

JWST: FIRST LIGHT, REIONIZATION & GALAXY ASSEMBLY

The HUDF data suggested that the LF at z ≳ 6 is very steep (Bouwens et al. 2010; Yan & Windhorst 2004b, et al. 2009), with a faint-end Schechter slope $|\alpha| \simeq 1.8$–1.9. This implies that dwarf galaxies may have collectively provided enough UV-photons to complete reionization at z≃6 (Yan & Windhorst 2004a). This assumes that the Lyman continuum escape fraction at z≃6 is as large as observed in Lyman Break Galaxies at z≃3, which is reasonable — although not proven — given the expected low dust content in dwarf galaxies at z≃6. HST/ACS has detect objects at z ≲ 6.5, and the new IR-channel on HST/WFC3 has been able to explore the redshift range z≃7–9 or 10 (Fig. 6a here; Bouwens et al. 2010, Yan et al. 2009).

Objects at z ≳ 9 are rare, since the volume element is small and JWST samples brighter part of LF. Fig. 6b shows that with proper survey strategy (area *and* depth), JWST can trace the entire reionization epoch from First Light at z≃20 (Cen 2003) to the end of the Reionization epoch at z≃6. JWST will detect the first star-forming objects (First Light star-clusters and subsequent dwarf galaxies), and measure their LF and its evolution. For this to be successful in realistic or conservative model scenarios, JWST needs to have the quoted sensitivity/aperture ("A"; to reach AB ≳ 31 mag or 1 nJy),

field-of-view (FOV=Ω; to cover GOODS-sized areas), and wavelength range (0.7–28 μm; to cover SED's from the Lyman to Balmer breaks at z $\gtrsim$ 6–20), as summarized in Fig. 6b. To study co-evolution of SMBH-growth and proto-bulge assembly for z $\lesssim$ 10–15 requires new weak AGN finding techniques for the JWST era, as we outlined here.

SUMMARY AND CONCLUSIONS

(1) Early-stage (major) mergers and faint variable objects have a redshift distribution similar to that of HUDF field galaxies, but there is very little overlap between the two.

(2) The peak in the epoch dependent density of major mergers may precede the peak in X-ray selected AGN density, but by no more than 1–2 Gyr.

(3) At z$\simeq$0.5–1.5, X-ray and radio selected galaxies are on average 0.5–1 Gyr older than the typical field galaxy age of 0.1–0.2 Gyr at the same redshift. *This suggests that AGN growth stayed in pace with galaxy assembly, but that the X-ray or radio selected AGN episode appeared $\lesssim$ 1 Gyr after the merger/starburst.* JWST will measure this in detail to AB $\lesssim$ 31 mag from 0.7–5.0 μm, tracing galaxy assembly and AGN & SMBH-growth since z $\lesssim$ 10–15. This requires new weak AGN finding techniques for JWST.

REFERENCES

51. Abraham, R. G., et al. 1996, MNRAS, 279, L47
51. Alexander, D. M. et al. 2003, AJ, 126, 539
51. Beckwith, S., et al. 2006, AJ, 132.1729
51. Bertin, E. & Arnouts, S. 1996, A&AS, 117, 363
51. Bouwens, R. J. et al. 2004, ApJL, 616, L79
51. Bouwens, R. J. et al. 2010, ApJ, 709, L133
51. Bruzual, G. & Charlot, S. 1993 ApJ, 405, 538
51. Cen, R. 2003, ApJ, 591, 12
51. Cohen, S. H., et al. 2003, AJ, 125, 1762
51. Cohen, S. H., et al. 2006, ApJ, 639, 731
51. Cohen, S. H., et al. 2010, ApJS, in prep.
51. Conselice, C. et al. 2004, ApJL, 600, L139
51. di Matteo, T., et al. 2005, Nature, 433, 604
51. Driver, S. P., et al. 1995, ApJL, 449, L23
51. Fan, X., et al. 2003, AJ, 125
51. Ferrarese L. & Ford H. 2004, SSR, 116, 523
51. Gardner, J., P., et al. 2006, SSR, 123, 485
51. Gebhardt, K., 2010, this Volume.
51. Glazebrook, K., et al. 1995b, MNRAS, 275, L19
51. Grazian, A., et al. 2004, AJ 127, 592
51. Hathi, N. et al. 2008, AJ, 135, 156
51. Hathi, N. et al. 2010, arXiv:1004.5141
51. Hopkins, P., et al. 2005, ApJL, 625, L71
51. Hopkins, P., et al. 2006, ApJS, 163, 1
51. Kogut, A., et al. 2003, ApJS, 148, 161
51. Komatsu, E., et al. 2010, arXiv:1001.4538
51. Kormendy, J. & Richstone, D. 1995, ARAA, 33, 581
51. Kormendy, J. & Gebhardt, K. 2001, AIP, 586, 363
51. Le Févre, O., et al. 2005, A&Ap, 439, 845
51. Lilly, S. J., et al. 1998, ApJL, 500, L75
51. Madau, P., & Rees, M. 2001, ApJ, 551, L27
51. Magorrian, J., et al. 1998, AJ, 115, 2285
51. Malhotra, S., et al. 2005, ApJ, 626, 666
51. Robertson, B., et al. 2005, ApJ, 632, 872
51. Ryan, R. E., et al. 2007, ApJ, 668, 839
51. Ryan, R. E., et al. 2008, ApJ, 678, 751
51. Ryan, R. et al. 2010, ApJ, subm. (arXiv:1006.xxxx)
51. Sarajedini, V. L., et al. 2003a, ApJ, 599, 173
51. Silk, J., & Rees, M. 1998, A&Ap, 331, L1
51. Springel, V., et al. 2005a, ApJ, 620, 79
51. Straughn, A. N., et al. 2006, ApJ, 639, 724
51. Szokoly, G. P., et al. 2004, ApJS, 155, 271
51. Vanzella, E. et al. 2005, A&A, 434, 53
51. White, S. & Rees, M. 1978, MNRAS 183, 341
51. Williams, R., et al. 1996, AJ 112, 1335
51. Windhorst, R. A., et al. 1991, ApJ, 380, 362
51. Windhorst, R. A., et al. 1998, ApJL, 494, L27
51. Windhorst, R. A., et al. 2006, New AR, 50, 113
51. Windhorst, R., e.a. 2010 ApJS (arXiv:1005.2776)
51. Yan, H., & Windhorst, R. 2004a, ApJL, 600, L01
51. Yan, H., & Windhorst, R. 2004b, ApJL, 612, L93
51. Yan, H., et al. 2009, arXiv:0910.0077